Ionization of Methane in Strong and Ultrastrong Relativistic Fields

Sasi Palaniyappan, Rob Mitchell, Rob Sauer, Isaac Ghebregziabher, Samantha L. White, M. F. Decamp, and B. C. Walker

Physics and Astronomy Department, University of Delaware, Newark, Delaware 19716, USA

(Received 18 December 2007; published 9 May 2008)

The photoionization of methane is reported for intensities up to 10^{19} W/cm^2 with linear and circular polarized light. While fragmental ions (e.g., CH_3^+, CH^+, C^+, C^{2+}) created from 10^{14} W/cm^2 to 10^{15} W/cm^2 are formed by Coulomb explosion, ionization to form C^{3+} and C^{4+} involves Coulomb explosion and tunneling ionization. In ultrastrong fields, removal of a carbon *K*-shell electron from methane proceeds via tunneling and rescattering ionization, without the influence of molecular channels. Photoelectrons from methane at 10^{19} W/cm^2 extend up to kinetic energies of 0.6 MeV.

DOI: 10.1103/PhysRevLett.100.183001 PACS numbers: 32.80.Rm, 33.60.+q, 33.80.Wz

The frontiers of high intensity laser science span an exceptional range of disciplines including plasma physics [1], fusion science [2], x-ray sources [3], atomic physics [4], and attosecond physics [5,6]. To date, molecules and clusters have been studied in strong (10^{14} W/cm^2 to 3×10^{16} W/cm^2) and ultrastrong (3×10^{16} W/cm^2 to 10^{19} W/cm^2) laser fields, respectively. Molecules in strong fields offer rich dynamics including molecular alignment [7,8], quantum control of reactions [9], ultrafast time resolution of dynamics [10], enhanced ionization [11,12], and Coulomb explosion (CE) [13,14]. For molecules and clusters in strong fields, photoelectrons are created with field ionization [15] shown in Figs. 1(a) and 1(b). As the interaction continues, additional dynamics are involved. Enhanced ionization [16] [Fig. 1(c)] occurs when the molecule expands in time (~ 100 femtoseconds) to a critical bond length (R_c) where excitation to highly ionized dissociative states is favorable. After initial field ionization, a molecule may also undergo rescattering ionization, where the photoelectron is driven back to the parent ion [17] by the oscillating laser field. Recently rescattering has been used to probe attosecond dynamics in molecules [18]. In clusters, further ionization proceeds via resonantly enhanced collision ionization [19] [Fig. 1(d)], where the photoelectrons gain energy from the field and collision ionize the cluster. The final dynamics in molecules and clusters is CE [Figs. 1(e) and 1(f)], where the system explodes into highly charged fragments. In nuclear fusion driven by CE of molecular clusters, one removes as many electrons as possible in an intense laser field before CE to achieve ~MeV fragmental kinetic energies. For example, in heavy methane cluster (CD_4) ionization, the highest charge state of C^{n+} one achieves before CE becomes important [20]. As the laser intensity is increased beyond that shown for molecules in Fig. 1(a), it is not known whether molecules will respond as independent ions or if collective mechanisms like CE continue to play a dominant role. Studies in molecules bridge a missing gap in ultrastrong field interactions, which to date have been measured in atomic systems, large clusters, and solid targets.

In this Letter, we report results for methane in linear (LP) and circularly polarized (CP) light fields from the onset of molecular ionization and CE to relativistic intensities. The intensity dependent data characterize the fundamental ionization yield and mechanisms behind the fragmental carbon ions from methane. Comparisons between fragmental ion production with LP and CP light indicate a transition from a strong field molecular CE response of methane to an atomiclike response in ultrastrong fields. This experimental observation is corroborated by comparisons to (1) ion production from an atomic carbon model and (2) the photoelectron spectra expected theoretically for atomic carbon.

Our experimental apparatus [21] consists of terawatt (90 mJ, 800 nm, 35 fs) and kilohertz (3 mJ, 790 nm, 45 fs) Ti:sapphire lasers, high resolution time-of-flight ion and electron spectrometers, and a magnetic deflection

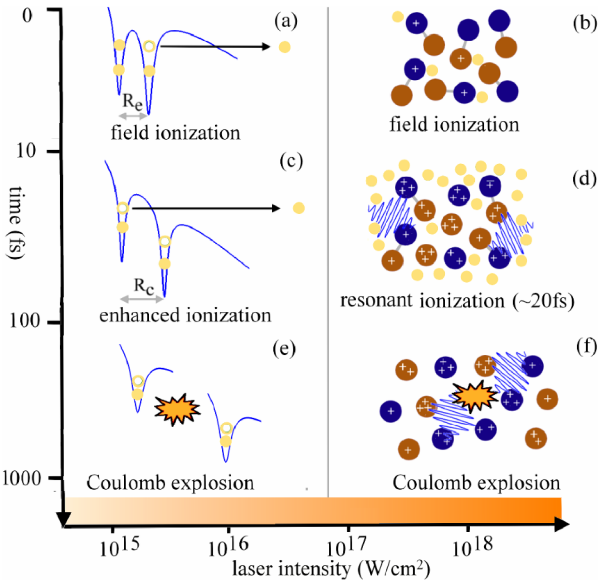

FIG. 1 (color online). Diatomic molecule and hetronuclear cluster ionization showing progression from field (a),(b) to enhanced or resonant ionization (c),(d) and CE (e),(f).

electron spectrometer. The high intensity was created by focusing the laser with an $f/2.7$ parabola in ultrahigh vacuum. A skimmed, effusive molecular beam of methane was crossed with the laser focus. In LP studies, the detector was perpendicular (parallel) to the laser polarization for ions (electrons). To eliminate mass degeneracies (e.g., $^{12}C^{4+}$:$^{12}CH_3{}^{5+}$) we used ^{13}C and ^{12}C. The data were averaged into 10% intensity bins and each data point represents typically three collections of 10^5 shots. Ionization saturated in the collections between 10^4 ions/shot-torr and 10^5 ions/shot-torr. The intensity is calibrated to 50% with measurements in krypton [4].

Figure 2(a) is a plot of the fragmental ion C^{2+}, C^{3+}, C^{4+}, and C^{5+} yields from methane in LP light across approximately a factor of a million in intensity and 8 orders of magnitude in signal. From the "knee" structure in the ion yields below saturation, one can see the ionization does not proceed from the detection threshold to saturation by a simple rate. At lower intensities, an analysis of the data shows the C^{3+}:C^{2+} ratio [Fig. 2(b)] is a constant 1:60 over 5 orders of magnitude in signal from 10^{-2} to 10^3 ions/shot-torr as the intensity increases from 1×10^{14} W/cm^2 to the saturation intensity of C^{2+} at 7×10^{14} W/cm^2. Such correlation between fragmental ions, whereby production saturates together and has the same intensity dependence, strongly implicates a common mechanism. Beyond C^{2+} saturation, a second process drives the C^{3+}:C^{2+} fragment ion ratio [Fig. 2(b)] up to 1:5 until C^{3+} production also saturates at 5×10^{15} W/cm^2. Consistent with the CE observed in previous studies [22–24], we, in fact, observe correlated production among several fragmental ions (e.g., $CH_3{}^+$, CH^+, C^+, and C^{2+}—not shown) for the ionization of methane from 1×10^{14} W/cm^2 to 7×10^{14} W/cm^2.

Moving to higher charge states, the C^{5+} knee structure spans from 10^{18} W/cm^2 down to the saturation intensity of C^{4+} (7×10^{15} W/cm^2). Several processes may contribute to this increased production including ionization [25] through resonant excitation, field driven rescattering ionization, and molecular mechanisms [Figs. 1(b) and 1(c)]. In CP fields, photoelectrons are driven away from the parent ion and mechanisms involving rescattering are greatly attenuated. Likewise, resonant excitations (though less likely to exist in ultrastrong fields) are affected by the laser polarization. CE, on the other hand, does not exhibit drastic sensitivity to the laser polarization since field ionization [Figs. 1(a) and 1(b)] is a function of the field magnitude.

To discern between possible ionization processes, we measured the carbon yields from methane in a CP field (Fig. 3). For comparison, the data in Fig. 2 are shown in Fig. 3 shifted by a factor of 1.4 to compensate for the lower peak field with CP. Ignoring the intensity shift, the C^{2+} and

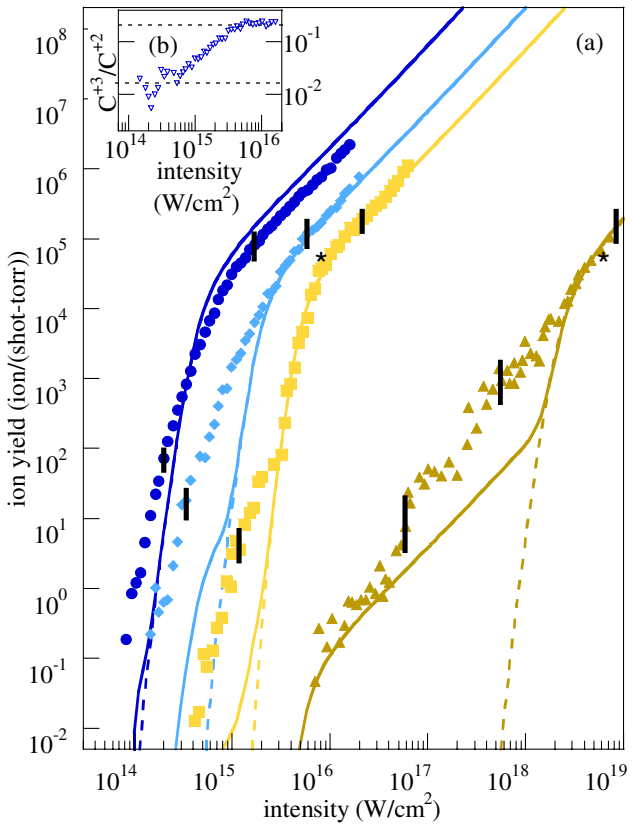

FIG. 2 (color online). C^{2+} (●), C^{3+} (◆), C^{4+} (■), and C^{5+} (▲) fragments with error bars from methane in LP light with calculated ADK (dashed lines) and total yields (solid lines) (a). Photoelectron collection intensities are noted (*). Inset (b) is the C^{3+}/C^{2+} production ratio (▽).

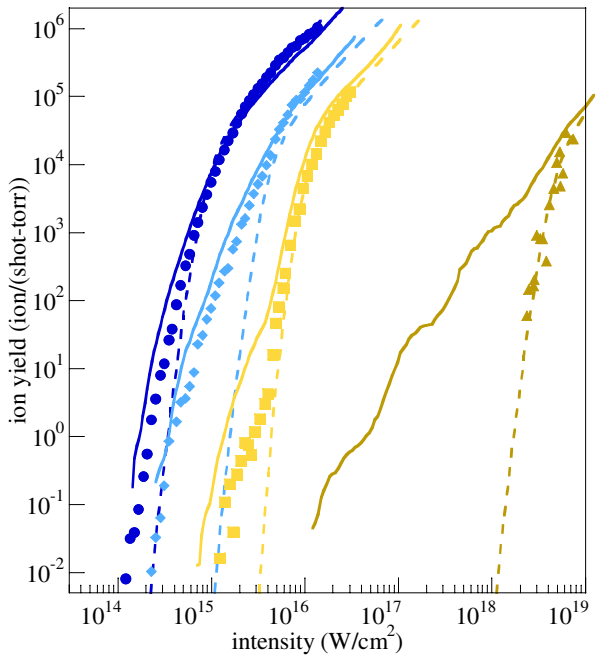

FIG. 3 (color online). C^{2+} (●), C^{3+} (◆), C^{4+} (■) C^{5+} (▲) from methane in CP light with the ADK model (dashed lines) and Fig. 2 LP yields (solid lines) of C^{2+} (blue), C^{3+} (light blue), C^{4+} (yellow), and C^{5+} (dark yellow).

C^{3+} yields for both polarizations are essentially the same—eliminating rescattering ionization or resonant excitation as a primary mechanism in the production of C^{2+} and C^{3+}. Progressing to C^{4+}, below 10 ion/shot-torr in Fig. 3 the yield still exhibits structure indicating an ionization mechanism that is not entirely rescattering. Closer examination shows C^{4+} from 1×10^{15} W/cm^2 to 5×10^{15} W/cm^2 is suppressed by a factor of 5 with CP when compared to LP. This partial attenuation with CP indicates the knee production of C^{4+} is due to two processes: rescattering and a collective excitation molecular mechanism, i.e., CE. Finally, for C^{5+} the evidence of a second rate giving rise to the knee structure is completely suppressed production CP light down to the 50 ions/shot-torr experimental limit. Within this limitation, the second component in the LP C^{5+} yield below 2×10^{18} W/cm^2 is suppressed by a factor of at least 50 with CP light, implicating the rescattering process.

Further insight on the interaction can be obtained from the photoelectrons. Figures 4(a) and 4(b) show the measured photoelectron spectra from methane at 8×10^{15} W/cm^2 and 7×10^{18} W/cm^2 for LP light. The decrease in the lower energy part of the spectra is partly due to the experimental collection. For Fig. 4(a) the collection below 200 eV is attenuated by stray magnetic fields and in Fig. 4(b) below 40 keV is limited by an aluminum filter before the detector. We note the 8×10^{15} W/cm^2 collection is nonrelativistic and along E, 90° from the laser k vector, while at 7×10^{18} W/cm^2 the interaction is relativistic and collected 65° from k toward E.

To better understand the production of fragmental ions from methane, we model field ionization, rescattering, and the photoelectron spectra using a semiclassical 3D relativistic model, described elsewhere [4]. Briefly, with the laser and focus parameters from the experiment, the model calculates field ionization using the tunneling ionization rate of Ammosov, Delone, and Krainov (ADK) [15] while approximating the carbon within methane as a free atom. As we will show, this approximation works well for higher charge states of carbon but does not address observations for C^+ or C^{2+} [26]. Following ionization, we use a trajectory ensemble to simulate the tunneling photoionization current, continuum dynamics, and rescattering of the photoelectron. The calculated photoionization current from a trajectory ensemble is shown in Fig. 5(a) as an example of the evolution and Lorentz deflection at 10^{17} W/cm^2 along the laser propagation direction (z) as a function of the time (t) after ionization until rescattering with the parent ion. Despite the 2 nm deflection away from the parent ion shown, the photoionization wave packet spread of ~8 nm still allows rescattering to occur.

The impact ionization cross sections used to calculate rescattering are given in Figs. 5(b) and 5(c). These cross sections, when multiplied by the rescattering flux from the photoionization current, give our calculated (e, ne) rate. $(e, 2e)$ and $(e, 3e)$ cross sections were obtained from experiments [27] and the Born-Bethe scaling law [4]. Excitation cross sections [27] were included for C^{3+} and C^{4+} assuming they lead to prompt ionization. We note while (e, ne) cross sections for methane ions have not been measured, the cross section for neutral methane to form C^+ is ~20% of the C to C^+ cross section [28]. Since the molecular bond influence on carbon is minimized for tightly bound electrons, the atomic rescattering approximation is expected to be most valid for C^{4+} and C^{5+} with impact energies above 100 eV.

The calculated total yields with LP, obtained by integrating the ionization rates over the laser pulse duration and laser focal volume, are plotted with the data in Fig. 2. As one can see in Fig. 2, the C^{3+}, C^{4+}, and C^{5+} yields from

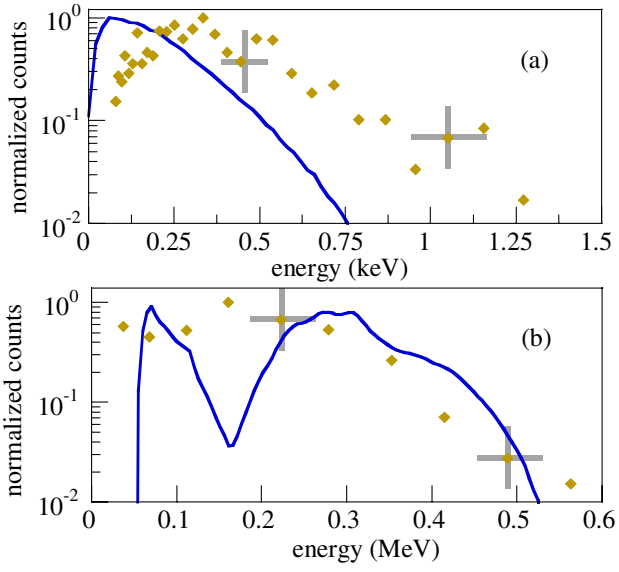

FIG. 4 (color online). Photoelectron spectra (◆) at 8×10^{15} W/cm^2 (a) and 7×10^{18} W/cm^2 (b) with the atomic theory (line) and error.

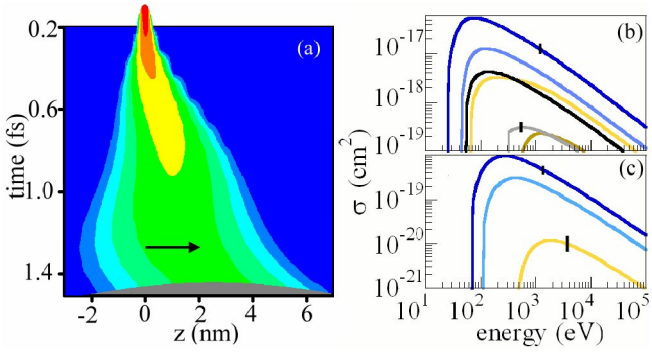

FIG. 5 (color online). Photoelectron current (C^{4+} at 10^{17} W/cm^2) from ionization (0.2 fs) to rescattering (1.5 fs), an arrow indicates Lorentz deflection (a). Cross sections with error bars for $(e, 2e)$ (b) and $(e, 3e)$ (c) in C^+ (blue), C^{2+} (light blue), C^{3+} (yellow), and C^{4+} (dark yellow) and excitation (b) in C^{3+} (black) and C^{4+} (gray).

methane agree well with the atomic carbon ADK near saturation. The deviation between the theory and the experiment for C^{2+} near and above saturation ($> 10^4$ ions/shot-torr) is due to the fact that this ionization proceeds by molecular tunneling [22–24]. The structure in the intensity dependent ion yields and deviations from the tunneling rate below saturation requires rates orders of magnitude greater than field ionization to begin to compare with the observed yields. With regard to this "nontunneling" yield below 10^3 ions/shot-torr, the atomic model accounts for between 1% and 2% of the measured C^{2+}, C^{3+} and C^{4+} from methane in a LP field, which is consistent with the ionization for these species tied primarily to molecular mechanisms. On the other hand, where the C^{5+} cross-shell ionization extends from the valence L shell to inner shell K electrons, the model accounts for 60% (9×10^{15} W/cm^2) to 15% (1.5×10^{18} W/cm^2) of the observed yields. Agreement of the rescattering ionization model with measured C^{5+} ion yields, coupled with the CP suppression, indicates C^{5+} ionization is atomic tunneling near saturation and involves cross-shell rescattering ionization [4] below saturation. As shown in Fig. 2, C^{5+} appears at 7×10^{15} W/cm^2 where the fragmental ion yields of C^{3+} and C^{4+} above saturation are in agreement with ADK.

A final analysis of the photoelectron spectra corroborates the ionization findings. Calculated photoelectron spectra with relativistically correct photoelectron propagation [29] are in excellent agreement [Fig. 4(b)] with our ultrastrong field experiments up to the rest mass of the electron. The dip at 150 keV not observed in the experiment may be attributed in part to the limited experimental energy resolution ($\Delta E/E = 0.3$), an oversimplification of the ADK model, or a deviation of the laser spatial mode from a perfect focus [29]. Overall the agreement between the data and atomic model, which essentially represents the ionization of C^{5+} in Fig. 4(b), substantiates the production of highly charged C^{5+} fragmentation with an atomiclike response rather than molecular. For completeness, we show in Fig. 4(a) the model results at lower intensities. The lack of agreement is most obvious for the keV energy photoelectrons in the experiment but lacking in the theory. Though one may suspect the intensity calibration, the disagreement is beyond the expected 50% uncertainty from the intensity calibration and the upper limit has already been used in the calculations. Some disagreement between the atomic carbon model and experiment is not unexpected since the formation of C^{4+} involves both molecular and atomic mechanisms.

In conclusion, we address how ionization proceeds for molecules in strong, nonrelativistic and ultrastrong, relativistic fields. We show C^{2+} ion from methane is produced through a molecular response; however, as one proceeds to C^{3+} and C^{4+} ions and the removal of the last two valence electrons, the ionization evolves from molecular mechanisms to an atomic response. Finally, for the ionization of the inner shell, the C^{5+} ions from methane are produced from an atomiclike response in an ultraintense field, including cross-shell rescattering ionization and a photoelectron spectrum in agreement with an atomic model. These results show atomic processes play a significant role in the production of highly charged fragmental ions beyond CE. Additional studies are underway to understand how this may be generalized to larger, nonsymmetric molecules.

This work is supported by the National Science Foundation (Grant No. 0457186) and the Delaware Space Grant College (Grant No. NNG05GO92H).

[1] J. Faure *et al.*, Nature (London) **444**, 737 (2006).
[2] S. Nakai and K. Mima, Rep. Prog. Phys. **67**, 321 (2004).
[3] K. Nakajima, Nature Phys. **4**, 92 (2008).
[4] S. Palaniyappan *et al.*, J. Phys. B **39**, S357 (2006).
[5] P. B. Corkum and F. Krausz, Nature Phys. **3**, 381 (2007).
[6] H. Kapteyn *et al.*, Science **317**, 775 (2007).
[7] B. Friedrich and D. Herschbach, Phys. Rev. Lett. **74**, 4623 (1995).
[8] H. Stapelfeldt and T. Seideman, Rev. Mod. Phys. **75**, 543 (2003).
[9] R. J. Levis, G. M. Menkir, and H. Rabitz, Science **292**, 709 (2001).
[10] H. Niikura *et al.*, Nature (London) **417**, 917 (2002).
[11] C. Guo, R. T. Jones, and G. N. Gibson, Phys. Rev. A **62**, 015402 (2000).
[12] A. J. Becker, A. Becker, and F. H. M. Faisal, Phys. Rev. A **69**, 023410 (2004).
[13] P. Hering and C. Cornaggia, Phys. Rev. A **59**, 2836 (1999).
[14] K. Zhao and W. T. Hill, Phys. Rev. A **71**, 013412 (2005).
[15] M. V. Ammosov, N. B. Delone, and V. P. Krainov, Sov. Phys. JETP **64**, 1191 (1986).
[16] K. Codling, L. J. Fransinski, and P. A. Hatherly, J. Phys. B **22**, L321 (1989).
[17] P. B. Corkum, Phys. Rev. Lett. **71**, 1994 (1993).
[18] S. Baker *et al.*, Science **312**, 424 (2006).
[19] T. Ditmire *et al.*, Phys. Rev. Lett. **78**, 2732 (1997).
[20] J. Jortner and I. Last, Chem. Phys. Chem. **3**, 845 (2002).
[21] A. DiChiara *et al.*, Opt. Lett. **28**, 2106 (2003).
[22] A. Talebpour *et al.*, Chem. Phys. Lett. **313**, 789 (1999).
[23] C. Wu *et al.*, J. Phys. B **35**, 2575 (2002).
[24] A. Sharifi *et al.*, J. Phys. Chem. A **111**, 9405 (2007).
[25] B. Walker *et al.*, Phys. Rev. A **48**, R894 (1993).
[26] Using C^+ to C^{3+} rates extracted from experimental yields or ADK does not sizably change C^{4+}, C^{5+} yields due to saturation of C^+ to C^{3+} where C^{4+}, C^{5+} rates are significant.
[27] NIFS DATABASE at https://dbshino.nifs.ac.jp.
[28] K. Gluch *et al.*, Int. J. Mass Spectrom. **228**, 307 (2003).
[29] A. Maltsev and T. Ditmire, Phys. Rev. Lett. **90**, 053002 (2003).